Scientia Iranica B (2019) 26(4), 2329–2341

Sharif University of Technology
**Scientia Iranica**
*Transactions B: Mechanical Engineering*
http://scientiairanica.sharif.edu

# Implementation of curved wall boundary and absorbing open boundary conditions for the D3Q19 lattice Boltzmann method for simulation of incompressible fluid flows

**E. Ezzatneshan***

*Aerospace Engineering Group, Department of New Technologies Engineering, Shahid Beheshti University, Tehran, P.O. Box 19839-9716, Iran.*

Received 28 January 2017; received in revised form 6 January 2018; accepted 23 June 2018

**KEYWORDS**
3-D lattice Boltzmann method;
Curved wall boundary condition;
Absorbing open boundary condition;
High Reynolds numbers;
Arbitrary geometries.

**Abstract.** In this study, a three-dimensional lattice Boltzmann method was developed for the numerical simulation of fluid flows around arbitrary geometries in a wide range of Reynolds numbers. For the efficient simulation of high Reynolds number flow structures in a turbulent regime, a Large Eddy Simulation (LES) approach with the Smagorinsky subgrid turbulence model was employed. An absorbing boundary condition based on the concept of sponge layer was improved and implemented to damp the vorticity fluctuations near the open boundaries and regularize the numerical solution by significantly reducing the spurious reflections from the open boundaries. An off-lattice scheme with a polynomial interpolation was used for the implementation of curved boundary conditions for arbitrary geometries. The efficiency and accuracy of the numerical approach presented were examined by computing the low to high Reynolds number flows around the practical geometries, including the flow past a sphere in a range of Reynolds numbers from $10^2$ to $10^4$ and flow around the NACA0012 wing section in two different flow conditions. The present results were found in good agreement with the numerical and experimental data reported in the literature. The study demonstrates that the present computational technique is robust and efficient for solving flow problems with practical geometries.



## 1. Introduction

In a wide range of applications with complex flow physics and geometries, the Lattice Boltzmann Method (LBM) is found to be a promising efficient technique for solving flow problems in comparison to conventional solvers based on the Navier-Stokes equations. The LBM is used to study the fluid flow with mesoscopic physics in which the interactions between particles are considered by a particle mass distribution function. The LBM is suitable for parallel computing due to the locality of the particle dynamics, which is parallel in nature. Furthermore, programming of the LBM is simple, and it is easy to model additional physical phenomena by using this method, considering the microscopic interactions. The standard LBM is applied to the uniform Cartesian grid and has a major restriction with respect to the curved boundary condition implementation. Further, the capability of this methodology to solve high Reynolds number flows may be trivial due to the inherent numerical instability. This instability comes from nonlinear flow features and, also, implementation of boundary conditions. The two

*. *Tel.: +98 21 29903244 (127)*
*E-mail address: e_ezzatneshan@sbu.ac.ir*

doi: 10.24200/sci.2018.20608

mentioned difficulties greatly limit the standard LBM applications to model practical flow problems with complex geometries. Thus, some efforts have been put forward to improve the efficiency and stability of the standard LBM.

The most common bounce-back method is used for applying the wall boundary condition in the LBM. The implementation of this method for curved boundary leads the LBM to be a scheme with only first-order accuracy in space because of a staircase-like approximation of the boundary [1]. The difficulty of employing conventional LBM for curved boundaries is tackled by introducing the immersed boundary method [2,3] and a family of boundary fitting methods proposed by Fillipova and Hänel [4], as improved by other researchers [5,6]. In the immersed boundary method, a local force computes the effect of the wall on the fluid, which is added by a source term to the governing equation. The existence of the forcing term in the LBM and immersed boundary approach impacts the stability of a numerical solution, thus is limited to using small CFL numbers.

In the boundary fitting approach, the lattice nodes inside and outside the fluid domain are considered as 'fluid nodes' and 'solid nodes', respectively. Then, to implement no-slip boundary condition on the curved wall, extrapolation of the velocity is used at the neighboring solid nodes, and the unknown distribution of the particles at the boundary nodes is defined by using the populations derived from fluid nodes. A similar procedure with very general formalism was derived by Lätt et al. [7], which can use both interpolation and extrapolation of the velocity at the boundary nodes. Verschaeve and Müller [8] extended Lätt's approach to curved boundary conditions, verified for the two-dimensional LBM; in this regard, thorough verification of the three-dimensional case is still necessary. In the present work, the approach proposed by Guo et al. [6] and Verschaeve and Müller [8] is extended and applied to three-dimensional LBM to solve practical fluid flows. Note that the application of an appropriate interpolation or extrapolation scheme to the implementation of the curved boundary conditions allows one to preserve spatial second-order accuracy of the LBM near the boundaries.

Different developments have been proposed to overcome the inherent instability of the standard LBM for solving flow problems at high Reynolds number. One way is to discretize the Lattice Boltzmann Equation (LBE) by using interpolation- or differential-type schemes [9-11]. These approaches eliminate the instability problem of the LBM by decoupling time and space discretizations [12]. Although these schemes provide a stable solution for LBM, the stencil used in discretizing the spatial derivatives sacrifices the locality of the collision of particles. Consequently, one of the main benefits of the LBM for efficient parallel computation is lost [13]. Another well-known approach to alleviating the stability limits of the LBM in solving high Reynolds number flows is to use the Multi-Relaxation-Time (MRT) [14,15] instead of the standard Single-Relaxation-Time (SRT) approach. The MRT approach allows selecting different values for the relaxation time parameter to keep the kinematic viscosity positive and, consequently, improve the numerical stability of the LBM. However, the MRT-based approach impacts the computational cost, especially for solving three-dimensional and practical flow problems.

One further idea to improve the stability of the LBM is to prevent the growth of the high-frequency spurious waves that usually originate from boundary conditions and nonlinear flow features in the flow domain. It is found that the implementation of boundary condition for the open boundaries strongly deteriorates the stability of the interior solution because of spurious wave reflections [16] in most of the numerical methods and the standard LBM. Non-Reflecting Boundary Conditions (NRBCs) have been developed to improve the numerical stability of the flow solutions by controlling the wave reflections from the boundaries. There are three main categories for NRBCs, including Characteristic Boundary Conditions (CBCs) [17,18], absorbing boundary condition based on the Perfectly Matched Layer (PML) concept [19,20], and the sponge layer concept [21,22]. These types of boundary conditions are successfully implemented to have stable numerical computing and realistic results based on the Navier-Stokes equations [17,19,21] and LBM [18,20,22].

Most of the previous LBMs developed in literature by implementing absorbing boundary conditions are used for solving aeroacoustic problems. The behavior of spurious reflections at open boundaries and their effects on the stability of LBM for high Reynolds number flows have been rarely considered. In the present work, the stability problem of the standard LBM with SRT-based approach and Bhatnagar-Gross-Krook (BGK) approximation for solving the high-Reynolds number flow problems is assessed by implementing absorbing boundary conditions in the outlet boundary. The application of this approach implies a stable solution through the standard LBM for solving the flow problems in a turbulent regime by absorbing the vorticity fluctuations, eliminating the spurious waves generated by nonlinear flow features, and preventing reflection to the interior solution domain. Herein, the concept of the sponge layer zone is employed to damp the reflecting spurious waves from the open boundaries. An improvement is also proposed for this approach, which is discussed in detail in Section 3. The LES methodology with the Smagorinsky subgrid model is used for turbulent flow simulations [23]. The accuracy

and efficiency of the D3Q19 SRT-lattice Boltzmann method implemented are investigated by solving incompressible flows around the practical geometries in different conditions. In the present paper, the stability and accuracy of the incompressible flow solver developed for solving flow problems in a wide range of Reynolds numbers are proved by implementing an off-lattice wall boundary condition for curved geometries and an absorbing boundary condition on the standard SRT-LBM with BGK approximation.

The paper is organized as follows: A brief introduction to the D3Q19 lattice Boltzmann single-relaxation-time method is presented in Section 2. Section 3 deals with the implementation of the curved boundary conditions with an interpolated off-lattice scheme. The application of the procedure of the sponge layer technique near the open boundaries is also described in Section 3. The numerical results of two flow problems are presented and discussed in Section 4 to examine the performance and accuracy of the solution of the LBM implemented. Finally, some conclusions are made in Section 5.

## 2. Numerical solution method

### 2.1. LBM for solution of laminar flows

The single relaxation time LB equation used with the collision term in the BGK approximation can be expressed as follows [24]:

$$\frac{\partial f}{\partial t} + e \cdot \nabla f = -\frac{1}{\tau}(f - f^{eq}), \tag{1}$$

where $f(t, c, x)$ is the particle (mass) distribution function, $\tau$ is the collision relaxation time, $e$ denotes the microscopic velocity of the particle, and $f^{eq}$ defines the equilibrium distribution function (the Maxwell-Boltzmann distribution function). The right-hand side of Eq. (1) (collision term) models the fluid viscosity effects on the molecular level through the collision process. A three-dimensional cubic lattice model with nineteen particle velocity directions (D3Q19) is employed to discretize Eq. (1) in the lattice configuration as follows:

$$\frac{\partial f_\alpha}{\partial t} + e_\alpha \cdot \nabla f_\alpha = -\frac{1}{\tau}(f_\alpha - f_\alpha^{eq}),$$
$$\alpha = 0, 1, ..., 18, \tag{2}$$

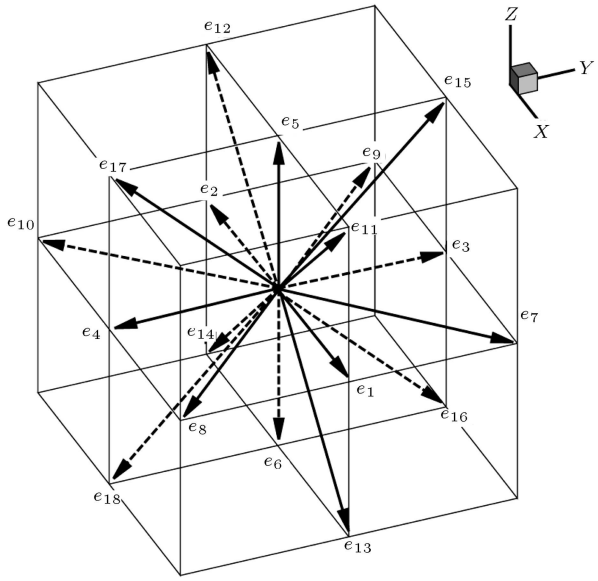


**Figure 1.** The cubic D3Q19 lattice model and the microscopic velocities.

where $\alpha$ denotes the possible direction of the particle velocity, $e$. Figure 1 indicates the directions of the discrete velocity, $e_\alpha$, for the D3Q19 discrete Boltzmann model employed, that are obtained by Eq. (3) shown in Box I, where $c = \Delta x/\Delta t$ is the lattice speed. $\Delta x$ and $\Delta t$ are the grid spacing and the time step size, respectively, which are assumed to be unity.

The equilibrium distribution function, $f^{eq}$, can be expressed as follows:

$$f_\alpha^{eq} = \rho w_\alpha \left(1 + 3\frac{e_\alpha \cdot \mathbf{u}}{c^2} + \frac{9}{2}\frac{(e_\alpha \cdot \mathbf{u})^2}{c^4} - \frac{3}{2}\frac{|\mathbf{u}|^2}{c^2}\right), \tag{4}$$

where $\mathbf{u} = (u, v, w)$ is the macroscopic velocity vector. The weight coefficient, $w_\alpha$, for the D3Q19 model is given by:

$$w_0 = \frac{1}{3}\ ,\quad w_{1-6} = \frac{1}{18}\ ,\quad w_{7-18} = \frac{1}{36}. \tag{5}$$

The macroscopic hydrodynamic variables such as fluid density $\rho$ and velocity $\mathbf{u}$ are obtained based on the distribution function with the following relations:

$$\rho = \sum_\alpha f_\alpha\ ,\quad \rho\,\mathbf{u} = \sum_\alpha e_\alpha\, f_\alpha. \tag{6}$$

$$e_\alpha = \begin{cases} (0,0,0) & \alpha = 0 \\ c(\pm 1,0,0),\ c(0,\pm 1,0),\ c(0,0,\pm 1) & \alpha = 1-6 \\ c(\pm 1,\pm 1,0),\ c(\pm 1,0,\pm 1),\ c(0,\pm 1,\pm 1) & \alpha = 7-18 \end{cases} \tag{3}$$

Box I

The pressure is defined by the state formula $p = \rho c_s^2$, where $c_s = c/\sqrt{3}$ is the sound speed [24]. The kinematic viscosity, $v$, depends on the speed of sound, $c_s$, and relaxation time, $\tau$, by the following definition:

$$v = c_s^2(\tau - 0.5). \tag{7}$$

The lattice Boltzmann equation discretized in Eq. (2) is usually solved in two steps: first, collision on the lattice nodes, known as 'collision step':

$$\overline{f}_\alpha(t,x) = f_\alpha(t,x) - \frac{1}{\tau}[f_\alpha(t,x) - f_\alpha^{eq}(t,x)], \tag{8}$$

second, propagation of the distribution $f_\alpha$ according to its respective speed known as 'free streaming step':

$$f_\alpha(t + \Delta t, x + e_\alpha) = \overline{f}_\alpha(t,x), \tag{9}$$

where $f_\alpha(t,x)$ and $\bar{f}_\alpha(t,x)$ denote the pre- and post-collision states of the distribution function, respectively.

### 2.2. LBM for solution of turbulent flows with LES approach

The LBM presented in the previous section has been used to accurately solve the fluid flows up to relatively moderate Reynolds number in a laminar flow regime. When the turbulent flow regime is achieved at high Reynolds number, a wide variety of temporal and spatial physical scales make such an approach computationally infeasible to obtain an efficient and accurate solution. The unresolved physical scales of turbulent motion by the governing equation are required to be captured by using an appropriate turbulence model. Many researchers have investigated the LBM in conjunction with Large Eddy Simulation (LES) approach to develop a suitable combination for simulation of the turbulent flows [23,25-27]. By applying this approach, the large-scale flow is solved exactly by the distribution function, $f$, and the influence of small-scale eddies is modeled through by computing the eddy viscosity, $v_t$. Therefore, the relaxation time, $\tau$, in the Boltzmann collision term in Eq. (2) should be modified to include both the molecular viscosity, $v_0$, and the eddy viscosity, $v_t$. Herein, the LES-LBE used is in the following form:

$$\frac{\partial f_\alpha}{\partial t} + \mathrm{e}_\alpha \cdot \nabla f_\alpha = -\frac{1}{\tau^*}(f_\alpha - f_\alpha^{eq}),$$

$$\alpha = 0, 1, ..., 18, \tag{10}$$

where the total relaxation time, $\tau^*$, is composed of two parts: the molecular relaxation time, $\tau_0$, depending on $v_0$ and the turbulence relaxation time, $\tau_t$, depending on $v_t$:

$$\tau^* = \tau_0 + \tau_t = \frac{(v_0 + v_t)}{c_s^2} + 0.5. \tag{11}$$

Herein, $v_t$ is computed by the Smagorinsky model as follows:

$$v_t = (C_s \Delta x)^2 \left|\overline{S}\right|, \tag{12}$$

where $C_s$ is the Smagorinsky model constant, which is set to 0.16 according to a sensitivity study in this work (see Table 3). The magnitude of the strain-rate tensor $\left|\overline{S}\right| = \sqrt{2\overline{S}_{ij}\overline{S}_{ij}}$ can be locally computed through the non-equilibrium momentum flux tensor, $\Pi^{neq}$, as follows:

$$\overline{S}_{ij} = -\frac{1}{2c_s^2\tau^*}\prod_{ij}^{neq}, \tag{13}$$

where $\prod_{ij}^{neq} = \sum_\alpha e_{\alpha i}e_{\alpha j}(f_\alpha - f_\alpha^{eq})$. Note that the LBM allows for direct computation of $|\bar{S}|$ using local variables, whereas the N-S-based solvers require an appropriate discretization procedure (like a finite-difference approximation) to evaluate $|\bar{S}|$. Finally, the same streaming-collision procedure discussed in the previous section is used to numerically solve the governing Eq. (10).

## 3. Boundary conditions

The implementation of curved wall boundary condition and absorbing open boundary condition is described in this section for the lattice Boltzmann method employed. For solving the LB equation numerically, it is required to determine appropriate boundary conditions for the distribution function, $f_\alpha$, based on the known macroscopic variables on each boundary.

For curved wall boundaries, the approach proposed by Verschaeve and Müller [8] is extended and applied to three-dimensional LBM. Herein, the neighboring nodes of the wall boundary are grouped into 'fluid nodes' inside the flow domain ($\mathbb{F}$), 'boundary nodes' near the wall ($\mathbb{B}$), and 'solid nodes' outside of the flow domain ($\mathbb{S}$). These groups are shown in Figure 2 by the black circle, gray circle, and square symbols, respectively. For the boundary node, N, in Figure 2, the populations of $\mathbb{F}$, $\mathbb{B}$, and $\mathbb{S}$ are as follows:

$$\mathbb{F} = \{2, 4, 5, 10, 12, 17\},$$

$$\mathbb{B} = \{0, 8, 9, 11, 14, 15, 18\},$$

$$\mathbb{S} = \{1, 3, 6, 7, 13, 16\}, \tag{14}$$

After streaming, the unknown populations for boundary node N would be $\{2, 4, 5, 10, 12, 17\}$, since they streamed from nodes outside the flow domain. Thus, those nodes are the opposite of the indices of the solid nodes $\mathbb{S}^{\text{opposite}} = \{2, 4, 5, 10, 12, 17\}$.

The macroscopic quantities $\mathbf{u}$ and $\rho$ are known after streaming on the fluid nodes, and the no-slip

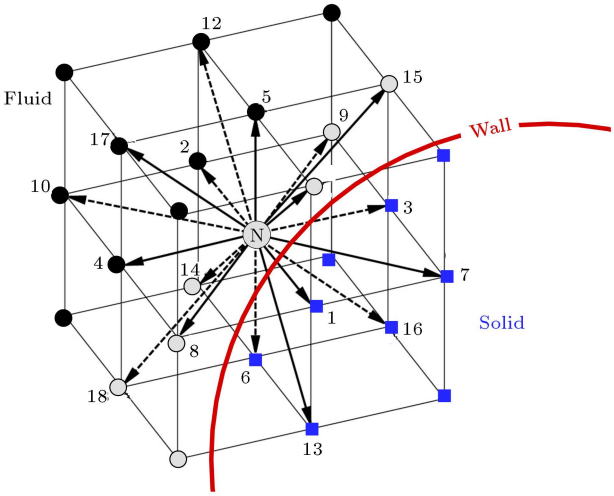


**Figure 2.** Close view of the boundary node N and its neighbors.

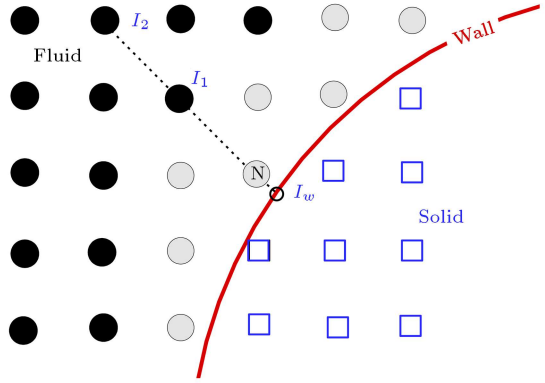


**Figure 3.** Approximating the macroscopic parameters at the boundary point N by an interpolating scheme along the dashed line.

boundary condition is imposed on the wall. The boundary nodes are placed between the fluid nodes and the wall. Therefore, the macroscopic properties of flow in the boundary nodes can be computed by an interpolation scheme, as will be discussed below.

### 3.1. Computing the velocity on the boundary nodes

The flow velocity components in the fluid nodes are computed after streaming through Eq. (6), and the wall velocity $\mathbf{u}_w$ is given by the velocity boundary condition (Dirichlet type). On the boundary nodes, however, the velocity is unknown because of unknown populations streamed in from the outside of the flow domain. As shown in Figure 3, the velocity, $\mathbf{u}_{\mathrm{N}}$, on the boundary node N of interest can be computed by interpolating the velocity between fluid nodes $I_1$, $I_2$ and the wall boundary condition at $I_w$. Herein, a quadratic Lagrangian interpolation scheme is used as follows:

$$\mathbf{u}_N = \mathbf{u}_w l_w + \mathbf{u}_1 l_1 + \mathbf{u}_2 l_2, \tag{15}$$

where $\mathbf{u}_w$, $\mathbf{u}_1$, and $\mathbf{u}_2$ are the velocity vectors at points $I_w$, $I_1$, and $I_2$, respectively. The interpolation polynomials $l_w$, $l_1$, and $l_2$ are evaluated as follows:

$$l_w = \frac{(d_{\mathrm{N}} - d_{I_1})(d_{\mathrm{N}} - d_{I_2})}{d_{I_1} d_{I_2}}, \tag{16}$$

$$l_1 = \frac{d_{\mathrm{N}}(d_{\mathrm{N}} - d_{I_2})}{d_{I_1}(d_{I_1} - d_{I_2})}, \tag{17}$$

$$l_2 = \frac{d_{\mathrm{N}}(d_{\mathrm{N}} - d_{I_1})}{d_{I_2}(d_{I_2} - d_{I_1})}, \tag{18}$$

where $d$ denotes the distance of the relevant node from the wall point, $I_w$. Note that these quantities can be computed once and for all in the first step of the solution.

### 3.2. Computing the density on the boundary nodes

A local algorithm is implemented to compute the density on the boundary node, N, based on the fact that the distribution functions are separable in $\rho$ such that it can be rewritten from Eq. (4):

$$f_\alpha^{eq} = \rho \underbrace{w_\alpha \left(1 + 3\frac{e_\alpha \cdot \mathbf{u}}{c^2} + \frac{9}{2}\frac{(e_\alpha \cdot \mathbf{u})^2}{c^4} - \frac{3}{2}\frac{|\mathbf{u}|^2}{c^2}\right)}_{g_\alpha^{eq}}. \tag{19}$$

Similarly, the non-equilibrium part can be approximated by the following relation [7]:

$$f_\alpha^{neq} \approx \rho \underbrace{\left(-\frac{3w_\alpha \tau}{c^2}(e_\alpha e_\alpha - \frac{3}{c^2}\mathbf{I}) : \mathbf{S}\right)}_{g_\alpha^{neq}}, \tag{20}$$

where $\mathbf{I}$ and $\mathbf{S}$ are the unit and rate of strain tensors, respectively. Then, by considering the mass of the post-streamed populations as approximately equal to the mass entering in collision, the density of the boundary node, N, can be approximated by:

$$\rho_N \approx \frac{\sum\limits_{\alpha \in \mathbb{K}} f_\alpha^{\mathrm{poststream}}}{\sum\limits_{\alpha \in \mathbb{K}} g_\alpha^{\mathrm{precoll}}}, \tag{21}$$

where $g_\alpha^{\mathrm{precoll}} = g_\alpha^{eq} + g_\alpha^{neq}$, and $\mathbb{K}$ includes the known population indices. Of note, to avoid possible numerical instability reported in [28], it is ensured that the known populations for node N in Eq. (21) include only those streamed from the fluid nodes around, not those from the neighboring boundary nodes.

### 3.3. Absorbing open boundary condition

As reviewed in the introduction, different non-reflecting boundary conditions have been developed for the N-S and LB-based flow solvers, most of which are applied to the solution of the aeroacoustic problems. These types of boundary conditions damp the unrealistic wave reflection from the boundary to improve the stability of the numerical solutions. Herein, a simple absorbing sponge layer approach is applied to keep the numerical algorithm as simple as possible. The idea behind this approach is to consider a layer of nodes near the open boundary, e.g., near the outlet boundary as shown in Figure 4, and then increase the viscosity artificially in that region. This sponge zone damps (absorbs) the waves entering this region because of the added viscosity and prevents those waves from reflecting on the open boundary to the entire domain. In the LBM, the relaxation time, $\tau$, imposes viscosity on the flow solution. Thus, this parameter should vary in order to add viscosity across the sponge layer considered by an appropriate relation. Vergnault et al. [22] proposed a quadratic relation to determine the relaxation parameter in a sponge layer as follows:

$$\tau_{\text{sponge layer}} = \begin{cases} \frac{3v+0.5}{1-0.999d^2} & d \le 1 \\ \frac{3v+0.5}{0.001} & d > 1 \end{cases} \quad (22)$$

where $d$ is the distance in a direction perpendicular to the open boundary. Such a quadratic relation produces an abrupt change in the viscosity across the interface of the fluid domain and the sponge layer, which may produce numerical errors. Herein, a sinusoidal relation is proposed and applied to evaluate the variation of the relaxation time in the interface between the fluid region and the sponge layer as follows:

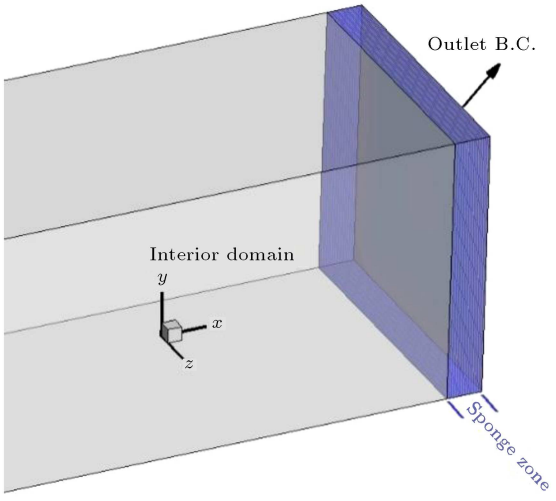


**Figure 4.** Schematic of the computational domain and the sponge layer considered near the outlet boundary condition.

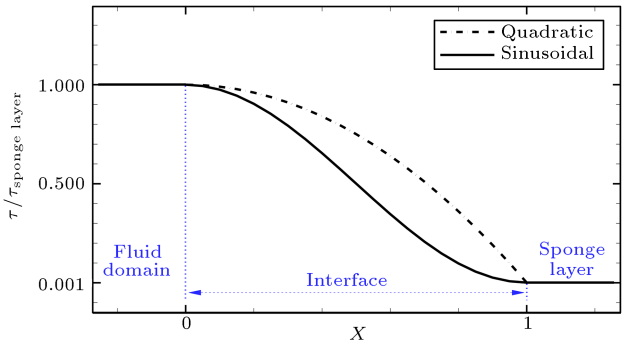


**Figure 5.** Variation of relaxation time parameter, $\tau$, in the interface between the fluid domain and the sponge layer.

$$\tau_{\text{interface}} = \frac{1+\frac{\tau}{\tau_{\text{sponge layer}}}}{2} + \frac{1-\frac{\tau}{\tau_{\text{sponge layer}}}}{2} \sin\left(\frac{2}{1-\frac{\tau}{\tau_{\text{sponge layer}}}} \frac{\frac{t_{\text{interface}}}{2} - t_{\text{interface}}}{\sigma}\right), \quad (23)$$

where $\tau/\tau_{\text{sponge layer}}$ is the relaxation time ratio between standard value and the desired value in the sponge layer. $t_{\text{interface}}$ denotes the width of the interface, and $\sigma$ is a scale parameter to set the rate of variations between $\tau$ and $\tau_{\text{sponge layer}}$ across the interface. Figure 5 shows the comparison of the quadratic and sinusoidal variations of the relaxation time in the interface between the fluid domain on the right and the sponge layer on the left. As shown in this figure, the sinusoidal variation is smoother than quadratic one in the interface, and it is expected to produce the least numerical errors. In this case, the width of interface and scale parameter are set to $t_{\text{interface}} = 1$ and $\sigma = 0.64$, respectively. The relaxation parameter is considered to vary from its standard value to 1000 times higher value across the sponge layer interface ($\tau/\tau_{\text{sponge layer}} = 0.001$). Note that by artificially adding such viscosity to the sponge layer, the relaxation time increases to a very large value such that the Chapman-Enskog expansion is no longer valid for that condition. As argued by Vergnault et al. [22], it is not important whether the physics in the sponge layer match just to dissipate energy.

## 4. Numerical results

The robustness and accuracy of the LBM implemented with D3Q19 discretization procedure are demonstrated for different laminar and turbulent flow problems with curved wall boundaries. Herein, two test cases include flow calculation past a sphere in a range of Reynolds numbers from $10^2$ to $10^4$ and flow around an NACA0012 wing section in different flow conditions. The present results obtained are compared with the available experimental data and numerical results reported in the literature.

### *4.1. Flow past a sphere*

The flow past a sphere is a well-known benchmark problem for the assessment of numerical methods due to the complicated 3-D flow structures and existence of numerous experimental and numerical results available in the literature for the sake of comparison [29-35]. The Reynolds number dramatically changes the nature of flow around the sphere. Applying an experimental investigation, Taneda [29] found that the flow past a sphere was perfectly laminar with no flow separation for the Reynolds numbers less than $\mathrm{Re} = u_0 D/v = 24$, where $u_0$ and $D$ are the freestream velocity and the sphere diameter, respectively. The flow is separated at the Reynolds number more than 25 from the rear stagnation point and forms recirculating wakes past the sphere. These wakes are in the shape of an axisymmetric vortex ring with steady behavior up to Reynolds number of approximately 210. However, the angle of flow separation point and the length of the wakes grow by increasing the Reynolds number. In the range of $210 < \mathrm{Re} < 270$, the laminar flow remains steady and attached; however, the wake is no longer axisymmetric. Magarvey and Bishop [31] considered this flow condition that exhibits planar symmetric wakes containing two vertical tails. As the Reynolds number increases within $270 < \mathrm{Re} < 400$, a transition from the steady laminar flow with planar symmetric wakes to a time-dependent laminar flow with periodic vortex shedding occurs. By increasing the Reynolds number up to $\mathrm{Re} = 1000$, an unsteady asymmetric regime is reported for the laminar flow past a sphere, where the formed vortex loops change from a cyclic mode to an irregular fashion [36]. The flow past a sphere with Reynolds numbers higher than $\mathrm{Re} > 1000$ is categorized in a turbulence regime with strong fluctuations existing in the wake. Taneda [30] and Achenbach [37] experimentally investigated the turbulent flow structures around a sphere in different Reynolds numbers, and showed that the vortex separation point rotated around the sphere at high Reynolds numbers.

The capability of the present solution procedure is proved in the process of simulating 3-D flow problems with curved boundaries by solving the flow past a sphere in a wide range of Reynolds numbers, $\mathrm{Re} = 100$, 200, $10^3$, and $10^4$. Figure 6 indicates the geometry of the solution domain consisting of a sphere confined in a cuboid with a square cross-section. The stream-wise length and height of the cuboid are $30D$ and $9D$, respectively. The sphere is placed in the middle of cross-section so that its center is at a distance of $4.5D$ from the inlet. Herein, the calculations are performed with the computational grid ($650\times200\times200$) for flows at $\mathrm{Re} = 100$, 200, $10^3$ and the grid ($975 \times 300\times300$) for $\mathrm{Re} = 10^4$. A sponge layer with $2D$ width is also considered to damp the vorticity fluctuations near the outlet boundary and stabilize the numerical solution, especially at high Reynolds numbers.

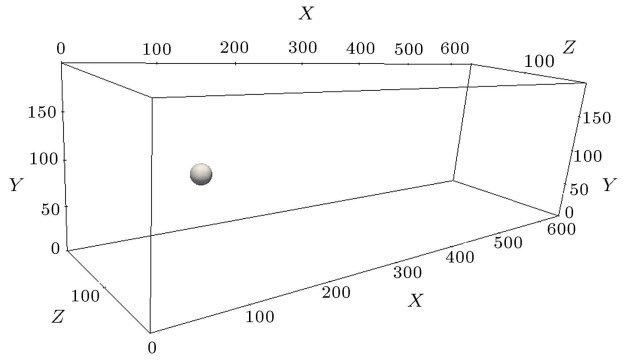


**Figure 6.** Cuboid computational domain implemented for simulation of flow past a sphere.

Figure 7 shows the 3-D computed flow field close to the sphere depicted by the streamlines (right) and the snapshot of an instantaneous velocity field in the computational domain (left) for $\mathrm{Re} = 100$, 200, $10^3$, and $10^4$, in descending order. A pair of axisymmetric stationary recirculating regions appears in the wake of the sphere at both the Reynolds numbers $\mathrm{Re} = 100$, and 200. As the Reynolds number increases from $\mathrm{Re} = 100$ to 200, the length of the ring vortex, $x_s$ (the distance from the rear stagnation point of the sphere to the end of the wake), increases and the separation angle, $\theta_s$, (measured from the front stagnation point) decreases. Table 1 shows the comparison of the computed results by applying the present LBM versus the available experimental data and numerical results regarding the separation angle and the location of the reattachment point for Re=100 and 200. As shown in this table, the present results by applying the D3Q19 LBM are compared well with the results reported in the literature. The irregular vortex shedding can be observed in Figure 7 with increasing the Reynolds number to $\mathrm{Re} = 10^3$. By increasing the Reynolds number to $\mathrm{Re} = 10^4$, the flow shows a chaotic nature resulting from vortex shedding, which is appropriately resolved by the LES-LBM implemented. This flow fashion is associated with the small-scale instabilities in the separated shear layer (the Kelvin-Helmholtz instability) and the large-scale instabilities in the wake. Figure 8 shows the mean surface pressure coefficient distribution obtained by employing the LES-LBM for the Reynolds number $\mathrm{Re} = 10^4$ in comparison with the experimental data [38] at $\mathrm{Re} = 1.62\times10^5$. The result obtained exhibits good agreement, and shows that the pressure distribution is almost independent of the Reynolds number in the subcritical regimes ($\mathrm{Re} \approx 10^5$) [38].

A further comparison of experimental and numerical results can be made with the drag coefficient, given as $C_d = \frac{8F_d}{\rho u_0^2 \pi D^2}$, where $F_d$ is the force on

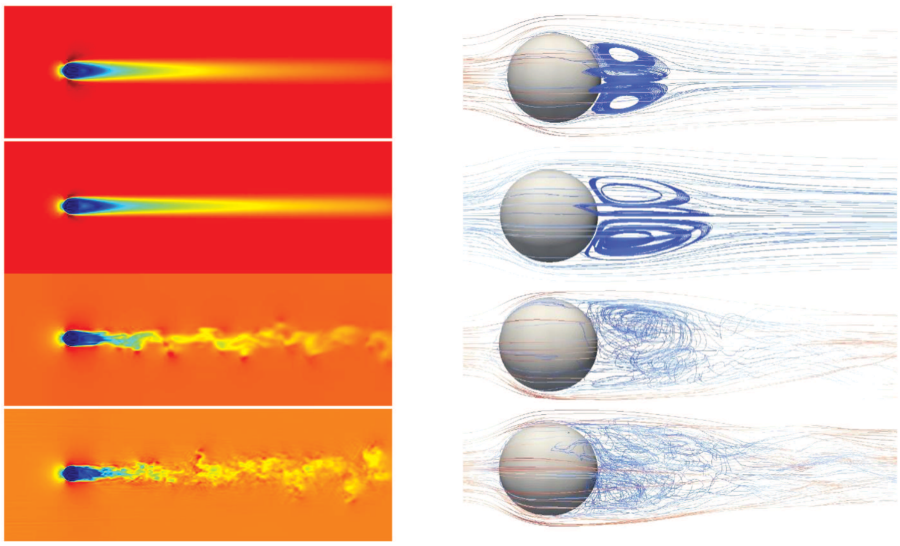

(a) (b)

**Figure 7.** Computed flow field for flow past a sphere shown by streamlines (a) and velocity contours (b) at Re = 100, 200, $10^3$, and $10^4$, in order from top to bottom.

**Table 1.** Comparison of the predicted separation angle and the location of the reattachment points for the flow past a sphere with Re = 100 and 200.

| Re | Author(s) | Method | $x_s$ | $\theta_s$ |
|---|---|---|---|---|
| 100 | Taneda [29] | Experiment | 0.89 | 127.6 |
| | Tomboulides [32] | Spectral Element | 0.86 | – |
| | Magnaudet et al. [33] | N.S. | 0.84 | – |
| | Johnson and Patel [34] | N.S. | 0.88 | 126.6 |
| | Present solution | LBM | 0.86 | 126.8 |
| 200 | Taneda [30] | Experiment | – | 116.8 |
| | Tomboulides [32] | Spectral Element | 1.43 | – |
| | Magnaudet et al. [33] | N.S. | 1.29 | – |
| | Johnson and Patel [34] | N.S. | 1.45 | 117.0 |
| | Present solution | LBM | 1.41 | 117.4 |

the sphere in the stream-wise direction. Herein, the drag force, $F_d$, is computed with the momentum-exchange method [39]. Table 2 shows the comparison of the results obtained from the LBM implemented and the available numerical results and experimental data for the mean drag coefficient of the sphere for Re = 100, 200, $10^3$, and $10^4$. The results obtained by applying the present solution approach are in good agreement with those reported in the literature. This study indicates that the LES-LBM can be used as a capable and accurate flow solver for simulating 3-D flow problems with curved wall boundaries, and that the results obtained are comparable to those of Navier-Stokes flow solvers.

The Smagorinsky constant, $C_s$, is an adjustable parameter [47], generally chosen to be around 0.15. However, this constant is experimented and analyzed in the present work to make an appropriate eddy viscosity prediction for the flow properties studied. Such a sensitivity study has been done for the flow around the sphere at Re = $10^4$ by applying the present LES-LBM. The comparison of the present results for the drag coefficient at different $C_s$ is given in Table 3. The results obtained show that by applying the present LBM, $C_s$ does not have significant effect on the numerical solution. Thus, $C_s = 0.16$ has been chosen as

**Table 2.** Comparison of the predicted drag coefficient for the flow past a sphere for different Reynolds numbers.

| Re | Author(s) | Method | $C_d$ |
|---|---|---|---|
| 100 | Roos & Willmarth [40] | Experiment | 1.08 |
| | Clift et al. [41] | Experiment | 1.087 |
| | Johnson and Patel [34] | N.S. | 1.08 |
| | Le Clair et al. [35] | N.S. | 1.096 |
| | Present solution | LBM | 1.091 |
| 200 | Tabata & Itakura [42] | N.S. | 0.77 |
| | Johnson and Patel [34] | N.S. | 0.77 |
| | Present solution | LBM | 0.772 |
| $10^3$ | Ploumhans et al. [43] | DNS | 0.48 |
| | Poon et al. [44] | LES-N.S. | 0.46 |
| | Present solution | LES-LBM | 0.496 |
| $10^4$ | Achenbach [37] | Experiment | $0.40 \pm 0.01$ |
| | Constantinescu et al. [45] | LES-N.S. | $0.393 \pm 0.014$ |
| | Poon et al. [44] | LES-N.S. | 0.39 |
| | Kim [46] | LES-N.S. | 0.438 |
| | Present solution | LES-LBM | $0.438 \pm 0.008$ |

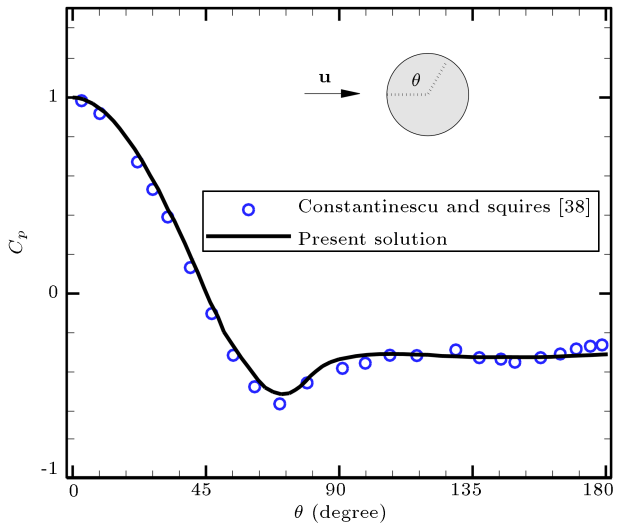


**Figure 8.** Comparison of mean surface pressure coefficient distribution for the sphere with $\mathrm{Re} = 10^4$.

an appropriate value for the Smagorinsky constant in the present work, which is close to the typical value of $C_s = 0.17$ used in the Navier-Stokes-based LES solvers [48].

The reduction of the spurious reflections from the outer boundary by the sponge layer is investigated for the flow around the sphere at $\mathrm{Re} = 10^4$. This study is performed by measuring the pressure wave reflection from the outlet boundary condition. Figure 9 shows the pressure fluctuation history measured in the middle of the flow domain point ($15D, 4.5D$, and $4.5D$), which is placed in the downstream of the sphere. In this figure, the results obtained by employing the sponge layer on the outlet boundary are compared with those obtained without using the sponge layer methodology. As can be observed, by considering the sponge layer in the outlet boundary condition, the pressure fluctuations are damped; the reflected wave is significantly weak compared to the condition where the sponge layer is not employed. This investigation demonstrates that the sponge layer has an effective role in stabilizing the numerical solutions based on the present LES-LBM by damping the waves reflected from the outlet boundary.

**Table 3.** Comparison of the predicted drag coefficient for the flow past a sphere at $\mathrm{Re} = 10^4$ for different Smagorinsky constants, $C_s$.

| $C_s$ | $C_d$ |
|---|---|
| 0.14 | $0.4379 \pm 0.0079$ |
| 0.16 | $0.4381 \pm 0.0083$ |
| 0.18 | $0.4381 \pm 0.0077$ |

### *4.2. Flow around a NACA0012 wing section*

Flows around the aerodynamic shapes are of complex nature and are characterized by the flow separation, reattachment, and unsteady shedding of vortices at low-to-high Reynolds numbers. These phenomena can

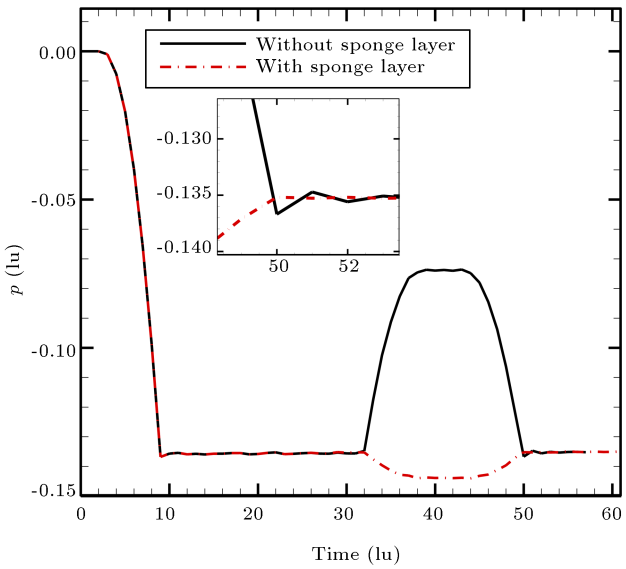


**Figure 9.** Comparison of pressure wave reflection in the middle of the flow domain, point ($15D$, $4.5D$, and $4.5D$), for the sphere with Re $= 10^4$.

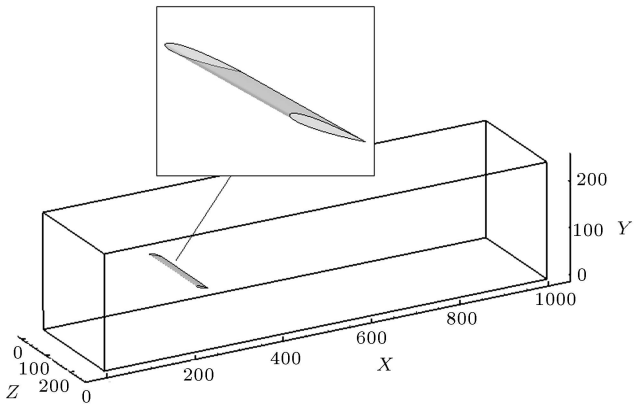


**Figure 10.** Geometry and the cuboid computational domain implemented for simulation of flow around the NACA0012 wing section.

impact the efficiency of the aerodynamic body (e.g., a wing) and, therefore, lead to different numerical and experimental studies regarding the prediction of such flow structures for improving engineering designs. Herein, the numerical simulation of the laminar and turbulent flows around an NACA0012 wing section is performed to examine the accuracy and performance of the D3Q19 LBM implemented. The Reynolds number, $\mathrm{Re} = u_0 c/v$, is defined based on the freestream velocity, $u_0$, and the chord length of the NACA0012 hydrofoil, $c$. The geometry of the NACA0012 wing section and the flow field with a grid size of $(1000 \times 250 \times 250)$ used for simulations are shown in Figure 10. The stream-wise and span-wise lengths of the cuboid flow domain are $40c$ and $10c$, respectively. The wing is placed in the middle of the cross-section so that its center is at a distance of $10c$ from the inlet. This study is performed with Re $= 500$ and $6 \times 10^6$ at angle-of-attack $\alpha = 10°$. The flow around the NACA0012 wing section used is quit laminar for Re $= 500$ and involves turbulent flow structures at Re $= 6 \times 10^6$. A sponge layer with $2c$ width is considered to damp the vorticity fluctuations near the outlet boundary condition at Re $= 6 \times 10^6$.

Figure 11 illustrates the computed results of flow structures around the NACA0012 wing section in the middle slice of the flow domain by the streamlines (right) and velocity contours (left) for Re $= 500$ (top) and $6 \times 10^6$ (bottom) at angle-of-attack $\alpha = 10°$. As observed in this figure, at the both Reynolds numbers, the flow separation occurs on the suction side of the wing, and large-scale vortexes are shed to downstream. In the case of Re $= 6 \times 10^6$, the flow is separated laminarly, and the transition to turbulence occurs on the separated shear layer along with vorticity fluctuations, which can be seen in the velocity field shown in Figure 11. In Figure 12, the surface pressure coefficient distribution calculated based on the present LBM employed is compared with the numerical results reported in [13,49] at Re $= 500$ and $\alpha = 10°$, showing good agreement. The time evolution of the drag and lift coefficients of the NACA0012 wing section are shown in Figure 13 for Re $= 6 \times 10^6$. In this figure, the periodicity can be observed, which corresponds to the large-scale vortex shedding from the separated shear layer. The mean values of drag and lift coefficients obtained are $C_d = 0.015$ and $C_l = 1.10$, respectively. The results obtained agree well with those reported by Haffman et al. [50], i.e., $C_d = 0.0144 \pm 30\%$ and $C_l = 1.11 \pm 5\%$. Validity and capability of the present solution algorithm are shown in this study for simulating the incompressible fluid flow field around the practical geometries.

## 5. Conclusion

In this work, a three-dimensional lattice Boltzmann method was developed for the numerical simulation of the fluid flows around the arbitrary geometries in a wide range of Reynolds numbers. The Large Eddy Simulation (LES) approach with the Smagorinsky subgrid turbulence model was employed to simulate high Reynolds number flow structures. An absorbing zone based on the concept of the sponge layer was implemented near the outlet boundary to damp the vorticity fluctuations and reduce the spurious wave reflections from the open boundary. An off-lattice scheme with a polynomial interpolation was also used to implement curved wall boundary conditions for the arbitrary geometries. The calculations were performed for different laminar and turbulent flow problems to demonstrate the efficiency and accuracy of the LBM

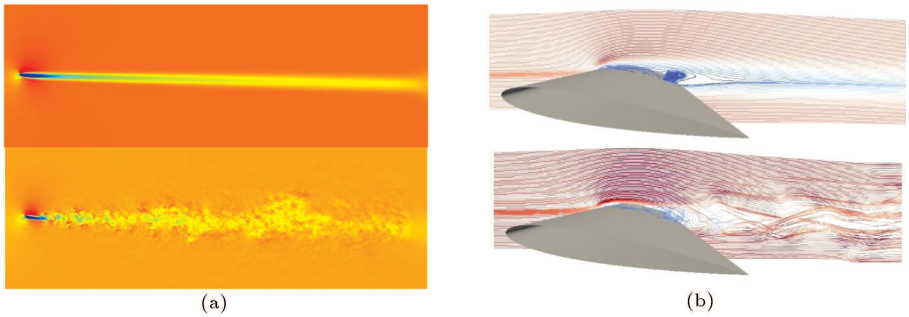


**Figure 11.** Computed flow field for flow around the NACA0012 wing section at $\alpha = 10^\circ$ shown by streamlines (a) and velocity contours (b) with $\mathrm{Re} = 500$ (top) and $\mathrm{Re} = 6 \times 10^6$ (bottom).

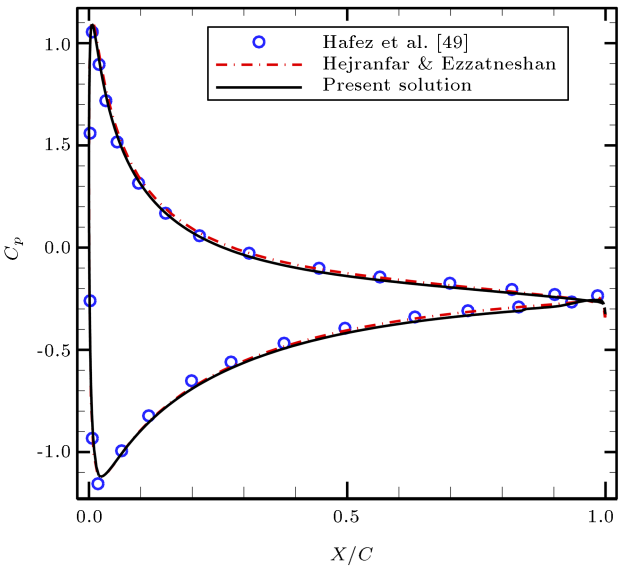


**Figure 12.** Comparison of surface pressure coefficient distribution in the middle of span of the NACA0012 wing section with $\mathrm{Re} = 500$ and $\alpha = 10^\circ$.

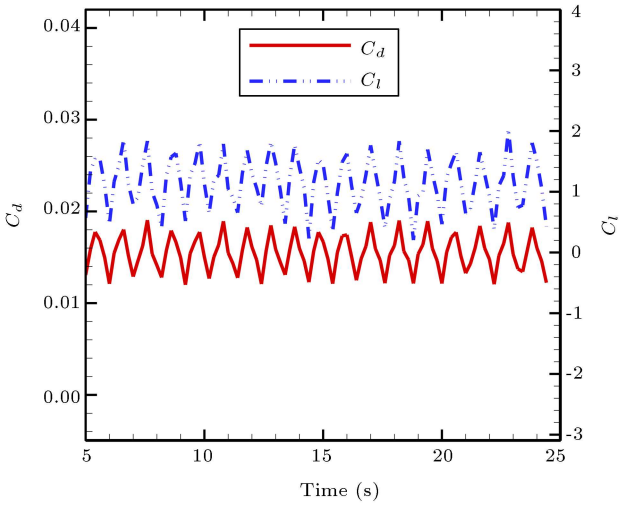


**Figure 13.** Time variation of drag and lift coefficients from flow around the NACA0012 wing section with $\mathrm{Re} = 6 \times 10^6$ and $\alpha = 10^\circ$.

applied. Some conclusions of the present study can be itemized as follows:

1. The off-lattice wall boundary condition proposed by Verschaeve and Müller for 2-D geometries was extended to the three-dimensional LBM using a Lagrangian polynomial interpolation and was examined by the simulation of the 3-D flow problems with curved wall boundaries. It was shown that such a procedure could accurately resolve the flow field near the curved wall boundaries;

2. For the implementation of the sponge layer near the outlet boundary, a sinusoidal relation was proposed to define a smooth variation for the relaxation time through the interface between the fluid domain and sponge layer to decrease probably numerical errors in this region. It was shown that the numerical solution of the high Reynolds number flows by the SRT-LBM and employing the sponge layer was robust and stable;

3. The computed results of implementing the LES-LBM were in good agreement with the available experimental data and numerical results reported in the literature for the test cases considered. The study showed that the present three-dimensional lattice Boltzmann method employed with the absorbing open boundary and curved wall boundary conditions was robust, efficient, and stable for solving fluid flows over practical geometries, even at high Reynolds numbers;

4. Results obtained based on the LES-LBM implemented were in good agreement with those of Navier-Stokes solvers. By considering the simplicity of the LBM for programming and its capability for parallel computing, it can be an appropriate alternative computational technique to the conventional Navier-Stokes solvers for studying physical phenomena and solving flow problems over practical and realistic geometries.

## Acknowledgment

The author would like to thank Shahid Beheshti University for the support of this research and the IPM for their high-performance computing service.

## References

1. Ginzbourg, I. and Adler, P.M. "Boundary flow condition analysis for the three-dimensional lattice Boltzmann model", *Journal de Physique*, **4**, pp. 191-214 (1994).
2. Shu, C., Liu, N., and Chew, Y. "A novel immersed boundary velocity correction-lattice Boltzmann method and its application to simulate flow past a circular cylinder", *Journal of Computational Physics*, **226**, pp. 1607-1622 (2007).
3. Navidbakhsh, M. and Rezazadeh, M. "An immersed boundary-lattice Boltzmann model for simulation of malaria-infected red blood cell in micro-channel", *Scientia Iranica B*, **19**(5), pp. 1329-1336 (2012).
4. Filippova, O. and Hänel, D. "Boundary fitting and local grid refinement for lattice-BGK models", *International Journal of Modern Physics C*, **9**, pp. 1271-1279 (1998).
5. Mei, R., Luo, L.-S., and Shyy, W. "An accurate curved boundary treatment in the lattice Boltzmann method", *Journal of Computational Physics*, **155**, pp. 307-330 (1999).
6. Guo, Z., Zheng, C., and Shi, B. "An extrapolation method for boundary conditions in lattice Boltzmann method", *Physics of Fluids*, **14**(6), pp. 2007-2010 (2002).
7. Lätt, J., Chopard, B., Malaspinas, O., Deville, M., and Michler, A. "Straight velocity boundaries in the lattice Boltzmann method", *Physical Review E*, **77**(5), p. 056703 (2008).
8. Verschaeve, J. and Müller, B. "A curved no-slip boundary condition for the lattice Boltzmann method", *Journal of Computational Physics*, **229**, pp. 6781-6803 (2010).
9. Guo, Z. and Zhao, T.S. "Explicit finite-difference lattice Boltzmann method for curvilinear coordinates", *Physical Review E*, **67**, p. 066709 (2003).
10. Hejranfar, K. and Ezzatneshan, E. "A high-order compact finite-difference lattice Boltzmann method for simulation of steady and unsteady incompressible flows", *Int. J. Numer. Meth. Fluids*, **75**, pp. 713-746 (2014).
11. Patil, V. and Lakshmisha, K.N. "Finite volume TVD formulation of lattice Boltzmann simulation on unstructured mesh", *Journal of Computational Physics*, **228**, pp. 5262-5279 (2009).
12. He, X. and Luo, L.-S. "Theory of the lattice Boltzmann method: from the Boltzmann equation to the lattice Boltzmann equation", *Physical Review E*, **53**, pp. 6811-6817 (1997).
13. Hejranfar, K. and Ezzatneshan, E. "Implementation of a high-order compact finite-difference lattice Boltzmann method in generalized curvilinear coordinates", *Journal of Computational Physics*, **267**, pp. 28-49 (2014).
14. McCracken, M.E. and Abaham, J. "Multiple-relaxation-time lattice-Boltzmann model for multiphase flow", *Physical Review E*, **71**, p. 036701 (2005).
15. Du, R., Shi, B., and Chen, X. "Multi-relaxation-time lattice Boltzmann model for incompressible flow", *Physics Letters A*, **359**, pp. 564-572 (2006).
16. Jung, N., Seo, H.W., and Yoo, C.S. "Two-dimensional characteristic boundary conditions for open boundaries in the lattice Boltzmann methods", *Journal of Computational Physics*, **302**, pp. 191-199 (2015). DOI: 10.1016/j.jcp.2015.08.044
17. hompson, K.W. "Time dependent boundary conditions for hyperbolic systems", *Journal of Computational Physics*, **68**(1), pp. 1-24 (1987).
18. Heubes, D., Bartel, A., and Ehrhardt, M. "Characteristic boundary conditions in the lattice Boltzmann method for fluid and gas dynamics", *Journal of Computational and Applied Mathematics*, **262**, pp. 51-61 (2014).
19. Hu, F. "A stable perfectly matched layer for linearized Euler equations in unsplit physical variables", *Journal of Computational Physics*, **173**, pp. 455-480 (2001).
20. Najafi-Yazdi, A. and Mongeau, L. "An absorbing boundary condition for the lattice Boltzmann method based on the perfectly matched layer", *Computers & Fluids*, **68**, pp. 203-218 (2012).
21. Bogey, C. and Bailly, C. "Three-dimensional non-reactive boundary conditions for acoustic simulations: far field formulation and validation test cases", *Acta Acustica United*, **88**, pp. 463-471 (2002).
22. Vergnault, E., Malaspinas, O., and Sagaut, P. "A lattice Boltzmann method for nonlinear disturbances around an arbitrary base flow", *Journal of Computational Physics*, **231**(24), pp. 8070-8082 (2012).
23. Koda, Y. and Lien, F.S. "The lattice Boltzmann method implemented on the GPU to simulate the turbulent flow over a square cylinder confined in a channel", *Flow, Turbulence and Combustion*, **94**(3), pp. 495-512 (2015).
24. Bhatnagar, P., Gross, E.P., and Krook, M. "A model for collision processes in gases i: small amplitude processes in charged and neutral one-component systems", *Physical Review E*, **94**, pp. 511-525 (1954).
25. Teixeira, C.M. "Incorporating turbulence models into the lattice-Boltzmann method", *Int. J. Modern Physics C*, **9**(8), pp. 1159-1175 (1998).
26. Krafczyk, M., Tolke, J., and Luo, L.S. "Large-eddy simulations with a multi-relaxation-time LBE model", *Int. J. Modern Physics B*, **17**(1), pp. 33-39 (2003).
27. Freitas, R.K., Schroder, W., and Meinke, M. "Investigation of lattice boltzmann methods for LES", *Progress in Turbulence II*, **109**, pp. 279-283 (2007).

28. Verschaeve, J.C.G. "Analysis of the lattice Boltzmann Bhatnagar-Gross-Krook no-slip boundary condition: ways to improve accuracy and stability", *Physical Review E*, **80**, p. 036703 (2009).

29. Taneda, S. "Experimental investigation of the wake behind a sphere at low Reynolds numbers", *J. Phys. Soc. Japan*, **11**, pp. 1104-1108 (1956).

30. Taneda, S. "Visual observations of the flow past a sphere at Reynolds numbers between $10^4$ and $10^6$", *J. Fluid Mech.*, **85**, pp. 187-192 (1978).

31. Magarvey, R.H. and Bishop, R.L. "Transition ranges for three-dimensional wakes", *Can. J. Phys.*, **39**, pp. 1418-1422 (1961).

32. Tomboulides, A.G. "Direct and large-eddy simulation of wake flows: flow past a sphere", PhD Thesis, Princeton University (1993).

33. Magnaudet, J., Rivero, M., and Fabre, J. "Accelerated flows past a rigid sphere or a spherical bubble, Part 1: Steady straining flow", *J. Fluid Mech.*, **284**, pp. 97-135 (1961).

34. Johnson, T.A. and Patel, V.C. "Flow past a sphere up to a Reynolds number of 300", *J. Fluid Mech.*, **378**, pp. 19-70 (1999).

35. Le Clair, B.P., Hamielec, A.E., and Pruppacher, H.R. "A numerical study of the drag on a sphere at low and intermediate Reynolds numbers", *J. Atmos. Sci.*, **27**, pp. 308-315 (1970).

36. Sakamoto, H. and Haniu, H. "A study of vortex shedding from spheres in uniform flow", *J. Fluids Eng.*, **112**, pp. 386-393 (1990).

37. Achenbach, E. "Experiments on the flow past spheres at very high Reynolds numbers", *J. Fluid Mech.*, **54**, pp. 565-575 (1972).

38. Constantinescu, G.S. and Squires, K. "LES and DES investigations of turbulent flow over a sphere at Re 10000", *Flow Turbulence and Combustion*, **70**, pp. 267-298 (2003).

39. Mei, R., Yu, D., Shyy, W., and Luo, L.-S. "Force evaluation in the lattice Boltzmann method involving curved geometry", *Physical Review E*, **65**(4), p. 041203 (2002).

40. Roos, F.W. and Willmarth, W.W. "Some experimental results on sphere and disk drag", *AIAA J.*, **9**, pp. 285-291 (1971).

41. Clift, R., Grace, J.R., and Weber, M.E., *Bubbles, Drops and Particles*, Academic Press, New York (1978).

42. Tabata, M. and Itakura, K. "A precise computation of drag coefficients of a sphere", *Int. J. Comput. Fluid Dynam.*, **9**, p. 303 (1998).

43. Ploumhans, P., Winckelmans, G.S., Slamon, J.K., Leonard, A., and Warren, M.S. "Vortex methods for direct numerical simulation of three-dimensional bluff body flow: Application to the sphere at Re = 300, 500, and 1000", *Journal of Computational Physics*, **178**, pp. 427-463 (2002).

44. Poon, E.K.W., Iaccarino, G., Ooi, A.S.H., and Giacobello, M. "Numerical studies of high Reynolds number flow past a stationary and rotating sphere", *7th International Conference on CFD in the Minerals and Process Industries*, CSIRO, Melbourne, Australia (2009).

45. Constantinescu, G.S., Chapelet, M.C., and Squires, K.D. "Prediction of turbulent flow over a sphere", *AIAA J.*, **41**, pp. 1733-1742 (2003).

46. Kim, S.E. "Large eddy simulation using unstructured meshes and dynamic subgrid- scale turbulence models", *34th AIAA Fluid Dynamics Conference and Exhibit*, Portland, Oregon, AIAA paper number 2004-2548 (2004).

47. Meyers, J. and Sagaut, P. "On the model coefficients for the standard and the variational multi-scale smagorinsky model", *J. Fluid Mechanics*, **569**, pp. 287-319 (2006).

48. Pope, S.B., *Turbulent Flows*, Cambridge University Press, Cambridge, UK (2000).

49. Hafez, M., Shatalov, A., and Nakajima, M. "Improved numerical simulations of incompressible flows based on viscous/inviscid interaction procedures", *Computers & Fluids*, **36**, pp. 1588-1591 (2007).

50. Hoffman, J., Jansson, J., and Jansson, N. "Simulation of 3D unsteady incompressible flow past a NACA 0012 wing section", Computational Technology Laboratory, Scientific and Technical Information Division, Report KTH-CTL-4023 (2012).

## Biography

**Eslam Ezzatneshan** is an Aerospace Engineer living and working in Tehran, Iran. He studied Aerospace Engineering and completed PhD ranked 1st at Sharif University of Technology, in 2014. He focused on numerical simulation of multiphase flows using the lattice Boltzmann method. Dr. Ezzatneshan obtained a post-doc position at Chalmers University of Technology in Sweden for 8 months in the same field of his expertise. Currently, he is an Assistant Professor in Shahid Beheshti University, Tehran, Iran. He works on developing solvers for numerical simulation of applied single- and multi-phase fluid flows using new computational techniques. The outcomes of his studies have been published in the several international journals, e.g., J. Ocean Engineering, J. Computational Physics, and Physical Review E.